Journal of Hazardous Materials 189 (2011) 827–835

Contents lists available at ScienceDirect

Journal of Hazardous Materials

journal homepage: www.elsevier.com/locate/jhazmat

Recovery of alumina and alkali in Bayer red mud by the formation of andradite-grossular hydrogarnet in hydrothermal process

Ran Zhang[a,b], Shili Zheng[a], Shuhua Ma[a,*], Yi Zhang[a]

[a] Key Laboratory of Green Process and Engineering, Institute of Process Engineering, Chinese Academy of Sciences, 100190 Beijing, China
[b] Graduate University of Chinese Academy of Sciences, 100049 Beijing, China

ARTICLE INFO

Article history:
Received 1 September 2010
Received in revised form 2 March 2011
Accepted 2 March 2011
Available online 9 March 2011

Keywords:
Bayer red mud
Andradite-grossular hydrogarnet
Hydrothermal process
Alumina
Alkali

ABSTRACT

Bayer red mud (RM) is an alumina refinery waste product rich in aluminum oxides and alkalis which are present primarily in the form of sodium hydro-aluminosilicate desilication product (DSP). A hydrothermal process was employed to recover alumina and alkali from "Fe-rich" and "Fe-lean" RM, the two representative species of RM produced in China. The hydrothermal process objective phase is andradite-grossular hydrogarnet characterized by the isomorphic substitution of Al and Fe. Batch experiments were used to evaluate the main factors influencing the recovery process, namely reaction temperature, caustic ratio (molar ratio of Na_2O to Al_2O_3 in sodium solution), sodium concentration and residence time. The results revealed that the Na_2O content of 0.5 wt% and A/S of 0.3 (mass ratio of Al_2O_3 to SiO_2) in leached residue could be achieved with Fe-rich RM under optimal conditions. However, the hydrothermal treatment of Fe-lean RM proved less successful unless the reaction system was enriched with iron. Subsequent experiments examined the effects of the ferric compound's content and type on the substitution ratio.

1. Introduction

As the world leader in alumina production, China's 23.79 million tonnes comprised nearly one-third of the global alumina output of 71.37 million tonnes in 2009 [1]. Bayer red mud (RM) is a solid waste produced during the process of extracting alumina from bauxite. Producing 1 tonne of alumina generates 1–1.5 tonnes of RM [2], depending on the quality of the source bauxite and the efficiency of the alumina extraction processes. It is standard practice to store this RM on land near the alumina refinery [3]. In 2009 China generated approximately 30 million tonnes of RM. Such large areas of land occupied by the solid waste storage not only carry a high financial cost but also present a significant contamination risk for neighboring communities, the local water supply, and any downwind areas. Responsibly managing these rapidly expanding solid waste stockpiles has become a serious problem for China.

Most alumina produced commercially from bauxite is obtained via the Bayer process [4]. The usual chemical compositions (% by wt) of RM resulted from Bayer process are Al_2O_3, 18–25; Na_2O, 8–12; SiO_2, 15–20; and TiO_2, 2–5 [5,6]. Fe_2O_3 and CaO are also present but their proportions vary greatly depending on the bauxite ore and leaching condition. Some alumina and alkali are lost during the Bayer leaching process when they combine with the silicon in bauxite to form DSP [7], an insoluble solid and the primary component of RM. RM's high alkalinity and the plentiful alumina fixed in its DSP make it a very attractive target for resource recovery efforts.

The DSP formed during the Bayer process takes two structures, sodalite and cancrinite [8]. The stoichiometry of sodalite and cancrinite has been reported as $Na_6[Al_6Si_6O_{24}]\cdot Na_2X\cdot nH_2O$, where X represents a variety of inorganic anions, most commonly CO_3^{2-}, SO_4^{2-}, $2Cl^-$, $2OH^-$ or $2NO_3^-$ [9]. Hence, the theoretical method for recovering alumina and alkali in RM was to destroy the structure of sodalite or cancrinite and to generate a new crystal phase lean in alumina and alkali. Following this guideline, the hydrochemical process proposed firstly by Ablamoff [10] was an effective method. Zhong et al. [11] went on to improve the reaction conditions and succeeded in recovering 87.8% of the Al_2O_3 and 96.4% of the Na_2O in RM. To recover alumina the hydrochemical process initially transforms DSP into $NaCaHSiO_4$. The $NaCaHSiO_4$ is then hydrolyzed to recover alkali. Though highly effective, this process requires two steps and the management of sodium concentrations as high as 35% Na_2O solution [11]. The hydrothermal process is relatively moderate. Cresswell and Milne [12] indicated that the hydrothermal process could achieve recoveries of 70% Al_2O_3 and 95% Na_2O under only 10–20% Na_2O solution and temperatures of 260–300 °C. Furthermore, the alumina and alkali could be recovered simultaneously in only one leaching step via the formation of silicate hydrogarnet.

The general chemical formula for silicate hydrogarnet is $\{X\}_3[Y]_2(SiO_4)_{3-x}(O_4H_4)_x$, where X and Y are cations [13]. X, Y and Si denote dodecahedral, octahedral and tetrahedral coordination relative to O, respectively [14]. The structure has the space

* Corresponding author. Tel.: +86 13521118758.
E-mail addresses: mashh27@126.com (S. Ma), zhangran1313@163.com (R. Zhang).

0304-3894/$ – see front matter © 2011 Elsevier B.V. All rights reserved.
doi:10.1016/j.jhazmat.2011.03.004

Table 1
Chemical compositions of RM (wt%).

	Na_2O	Al_2O_3	Fe_2O_3	SiO_2	CaO	TiO_2	A/S
Fe-rich RM	10.46	21.49	22.13	18.46	6.89	3.14	1.16
Fe-lean RM	8.22	23.80	6.46	18.97	18.00	5.16	1.25

group *Ia3d* and all cation positions are fixed by symmetry [15]. Its structure has been described as one of the considerable chemical compliance which can accommodate a wide variety of elements. These site occupancies involve Na, Mg, Ca and so on in X-site; Al, Fe, Mg, Ti and so on in Y-site [16]; and the mutual substitution of $(SiO_4)^{4-}$ and $(O_4H_4)^{4-}$ [17,18]. Consequently, many species of silicate hydrogarnet with isomorphic substitution always exhibit extensive solid solution.

The silicate hydrogarnet reported in the hydrothermal process has the chemical formula $Ca_3[Al,Fe]_2(SiO_4)_{3-x}(O_4H_4)_x$, which occurs with the isomorphic substitution of Al and Fe [19]. This silicate hydrogarnet is the solid solution of andradite-grossular hydrogarnet, of which prototypes are $Ca_3Fe_2(SiO_4)_{3-x}(O_4H_4)_x$ and $Ca_3Al_2(SiO_4)_{3-x}(O_4H_4)_x$, respectively. Obviously, andradite hydrogarnet contains no sodium theoretically, and little aluminum depending on the extent of iron substitution. Hence, it is a kind of ideal phase of the residue in alumina production.

Zoldi et al. [19] and Li et al. [20] investigated the generation of silicate hydrogarnet during the digestion of bauxite. Owing to the addition of lime, the sodium content in RM decreased significantly. However, because it was restricted by the Bayer process' caustic ratio (molar ratio of Na_2O to Al_2O_3 in sodium solution), the extent of iron substitution proved undesirable and lead to the A/S RM ranging from 0.71 to 1.53 [20]. Here again, treating RM via silicate hydrogarnet generation through the hydrothermal process is promising because of the distinct difference in caustic ratio between the hydrothermal and Bayer processes. Cresswell and Milne [12] and Solymar et al. [21] achieved ideal results when treating RM by the hydrothermal process. However, their work did not account for the real-world heterogeneity of RM, which typically has a widely varying chemical composition and characterization due to the bauxite ore used and leaching conditions.

Bauxite is composed of one or more aluminum hydroxide minerals, including primarily gibbsite, boehmite and diaspore. There are also other compounds such as hematite, goethite, quartz, rutile/anatase, kaolinite and other impurities in minor or trace amounts. China is abundant with bauxite reserves mainly in the form of diaspore. The Bayer process has been successfully applied in China for local diaspore ore, as well as in more and more plants for imported gibbsite-bauxite from Indonesia, Australia, Vietnam, and others [3].

Extraction from diasporic-bauxite requires higher temperatures and sodium concentrations than those needed for gibbsite and boehmite. Moreover, Chinese bauxite samples are iron-poor compared with ores from Australia and Indonesia [3]. These differences, coupled with the fact that just over half of the bauxite processed in China in 2008 was imported, have led to the existence of two distinct kinds of RM in China.

In this paper, the two aforementioned kinds of RM were run through the hydrothermal process to determine the effect RM species has on the formation of silicate hydrogarnet. In addition, the iron content and type in RM with respect to the replacement of silicate hydrogarnet in the case of aluminum and iron were also researched. Owing to the uncertainty of the formula of garnet [16,22], end-member minerals were used to define garnet components. Following the characteristics of an end-member described by Hawthorne [22], three crystal phases were selected according to their XRD patterns to define the solid solution of andradite-grossular hydrogarnet in this study.

2. Experiment

2.1. Raw materials

In this study, the two predominant kinds of RM found in China were subject to experimentation – Fe-rich and Fe-lean RM sourced from Shandong and Henan Province, China, respectively. The Fe-rich RM was generated from imported gibbsite-bauxite by the orthodox Bayer process, while the Fe-lean RM was generated from local diaspore-bauxite by the improved Bayer process. Their chemical compositions are shown in Table 1.

According to the XRD pattern shown in Fig. 1, the identified mineral phases of DSP are $1.08Na_2O{\cdot}Al_2O_3{\cdot}1.68SiO_2{\cdot}1.8H_2O$ and $Na_8(AlSiO_4)_6(OH)_2{\cdot}4H_2O$ – both of them belong to sodalite. In Fe-rich RM, iron appears in the form of hematite and goethite, while it takes the form of andradite-grossular hydrogarnet $Ca_3AlFe(SiO_4)(OH)_8$ in Fe-lean RM owing to the higher tempera-

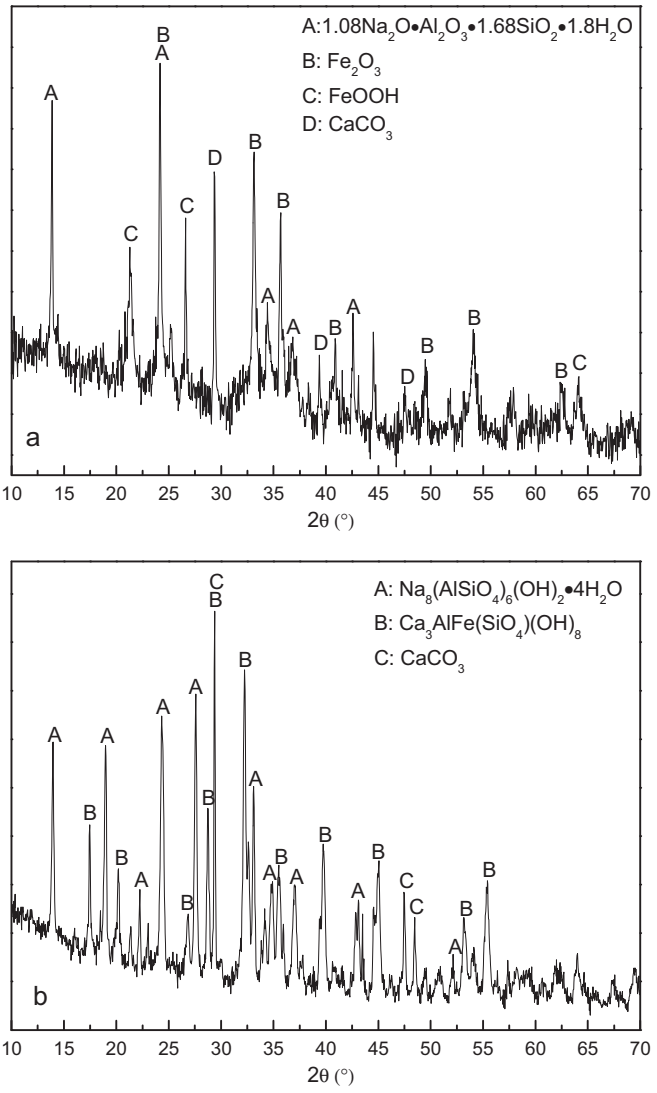

Fig. 1. XRD patterns of Fe-rich RM (a) and Fe-lean RM (b).

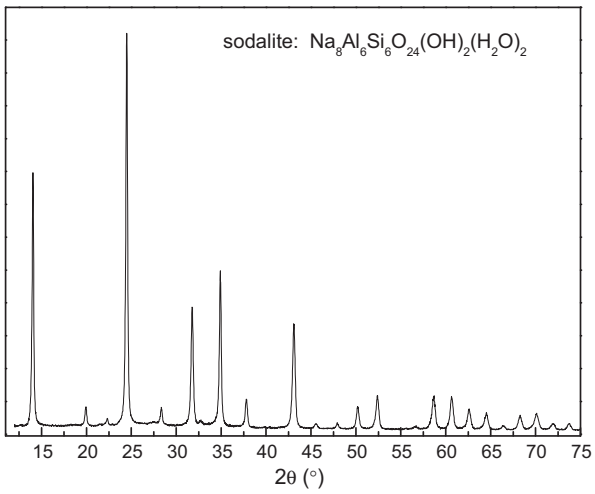

Fig. 2. XRD pattern of synthetic sodalite.

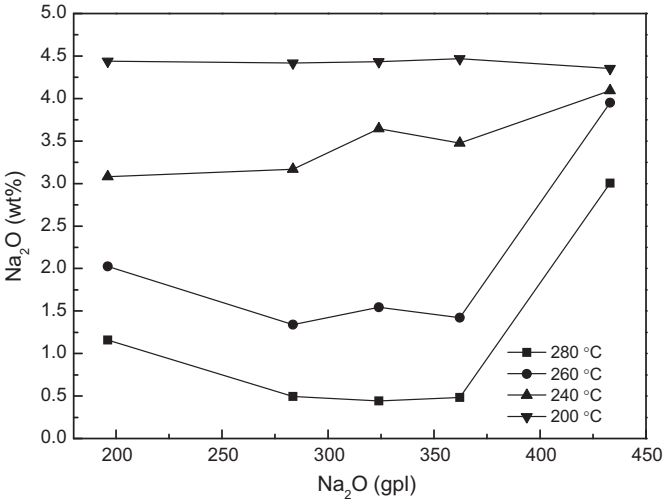

Fig. 3. Na_2O content in leached Fe-rich RM as a function of sodium concentration.

ture and sodium concentration during digestion. In RM, Ti always exists in the form of calcium–titanium compounds [23]. However, no Ti-bearing compounds are scrutinized in the XRD patterns.

These two kinds of RM were prepared for 24 h in an oven at 80 °C, and then grinded to sieve for 100 mesh.

Sodalite was synthesized in this study in order to investigate the phase transition. The synthetic was acquired from analytically pure samples of chemical reagents NaOH, $Al(OH)_3$, $Na_2SiO_3{\cdot}9H_2O$, and $Ca(OH)_2$.

A 2 l high-pressure autoclave fitted with an external heater and an internal cooling system was used to synthesize sodalite. The autoclave is protected by a nickel vessel from corrosion due to the high alkali solution. An automatic proportional, integral and derivative (PID) control system managed the heating rate, agitation, and temperature of the autoclave.

According to the operating conditions of bauxite digestion, the synthesis of sodalite was carried out at 200 °C for 2 h in the autoclave. The sodium aluminate solution was prepared by Na_2O, 196 gpl and caustic ratio 1.5. And then reagent $Na_2SiO_3{\cdot}9H_2O$ was added into solution to make the calculated concentration of SiO_2 (assuming that SiO_2 dissolves in solution entirely) reach 150 gpl. Table 2 shows the synthetic solid's chemical composition and Fig. 2 displays its XRD pattern. The synthetic solid was ground and sieved through 100 mesh for subsequent use.

2.2. Experimental operations

The study was composed of two parts: (a) The hydrothermal process was applied to Fe-rich and Fe-lean RM at various leaching temperatures, sodium concentrations, caustic ratios and residence times to explore the recovery rates of alumina and alkali as well as the differences in DSP to silicate hydrogarnet transformation. (b) The influence of iron content on recovery rates was analyzed by adding ferric compound to synthesized sodalite. The effect of the ferric compound's type was also researched.

These experiments were carried out in 200 ml parr autoclaves with pure nickel protective linings. These parr autoclaves were fixed inside a temperature and rotation speed controlled incubator. After reaction, the slurry was filtered and then twice washed with deionized water at 80 °C for 10 min before finally being dried for 10 h in an oven at 80 °C. The leached residues were subjected to X-ray diffraction (X'Pert Pro MPD of Panalytical Company, 40 kV, 30 mA, Cu Kα as X-ray source) for identification of crystalline phases. The chemical components of the leaching liquor and leached residues were analyzed by ICP-OES (Optimal 5300DV of PerkinElmer Instruments, 1300 W, carrier gas flow 0.08 l/min, peristaltic pump flow 1.5 ml/min).

The main test parameters for the hydrothermal treatment of RM are as follows:

Temperature: 200–280 °C.
Sodium concentration (as Na_2O): 196–433 gpl
Initial caustic ratio: 5–infinity.
CaO dosage, CaO-to-SiO_2 mole ratio in RM: 1.5 (including the CaO in RM).
Residence time: 20–240 min.
Liquid-to-solid mass ratio: 8.

Table 2
Chemical compositions of synthetic sodalite.

Composition	Na_2O	Al_2O_3	SiO_2
Content (wt%)	20.24	21.06	25.45

3. Results and discussion

3.1. Hydrothermal process for Fe-rich and Fe-lean RM

3.1.1. Dealing with Fe-rich RM

3.1.1.1. Effects of sodium concentration and temperature. These experiments were carried out at caustic ratio 20, residence time 2 h with various sodium concentrations and temperatures. Figs. 3 and 4 show the fluctuation of Na_2O content and A/S in leached RM as sodium concentration increases. The Na_2O content and A/S decreased monotonically as temperature increased, with high temperature markedly enhancing the extraction of alumina and alkali. The variation trend of Na_2O content versus sodium concentration can be neatly divided into two parts according to operating temperature. While changing little at relatively low temperatures (200, 240 °C), Na_2O content decreased slowly before rapidly increasing at relatively high temperatures (260, 280 °C).

A/S in leached residue only changed slightly across various sodium concentrations. The alumina content decreased gradually as temperature increased, ultimately reaching 5 wt% at 280 °C as listed in Table 4. The A/S in leached solution decreased with sodium concentration or temperature increasing. These observations are explained by the fact that the solubility of silicon increases with increasing sodium concentration and temperature [8], a relationship which results in only the fluctuation of A/S recorded in both leached residue and solution.

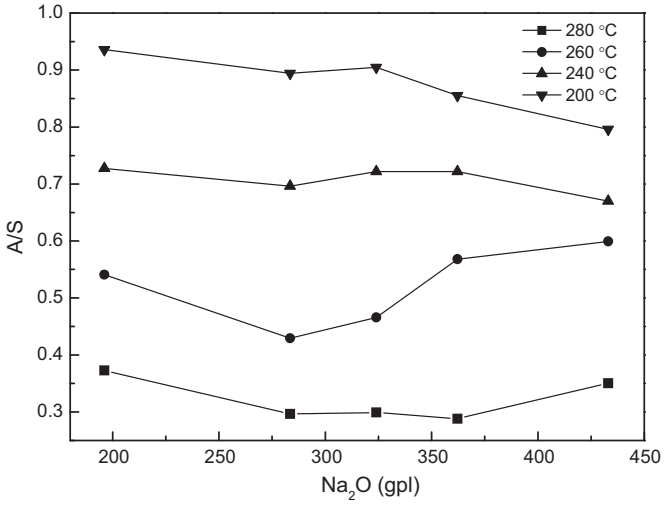

Fig. 4. A/S in leached Fe-rich RM as a function of sodium concentration.

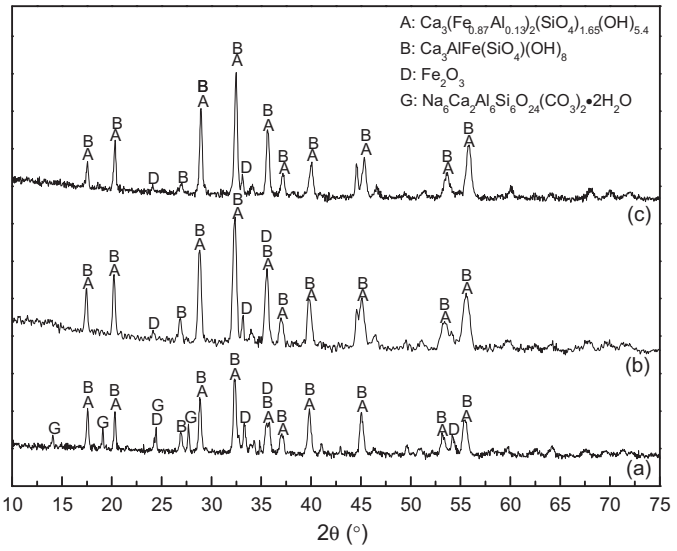

Fig. 5. XRD patterns of leached Fe-rich RM after leaching at sodium concentration 324 gpl and different temperatures: (a) 200 °C, (b) 240 °C, (c) 280 °C.

Based on the results above, it is under the conditions of 280 °C and Na_2O 283–362 gpl that the Na_2O content and A/S in leached residue can reach minimum, approximately 0.5 wt% and 0.3, respectively.

3.1.1.2. Analysis of phases. Figs. 5 and 6 show several XRD patterns from these experiments. The silicate hydrogarnet generated in the reaction appears as $Ca_3(Fe_{0.87}Al_{0.13})_2(SiO_4)_{1.65}(OH)_{5.4}$ (1#) and $Ca_3AlFe(SiO_4)(OH)_8$ (2#). The PDF (Powder Diffraction File) numbers for these XRD patterns are 87-1971 and 32-0147, respectively. Owing to their isomorphic structure, it is difficult to discern

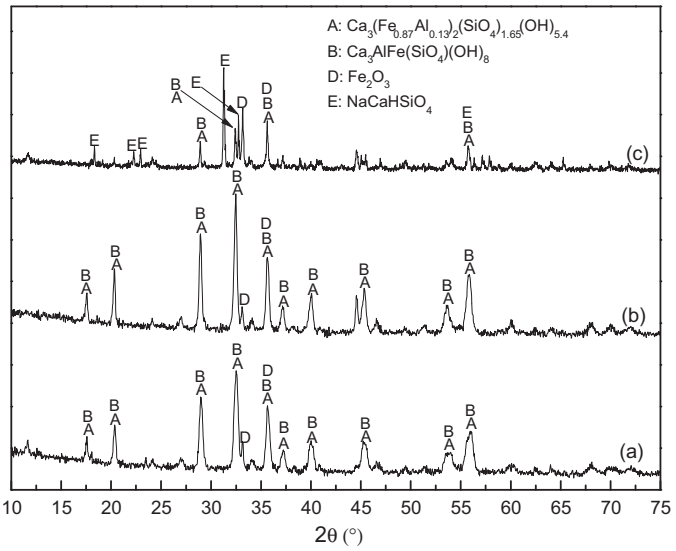

Fig. 6. XRD patterns of leached Fe-rich RM after leaching at 280 °C and different sodium concentrations: (a) 196 gpl, (b) 324 gpl, (c) 433 gpl.

the difference between them. However, the leached RM's A/S values listed in Tables 3 and 4 fall in between those of 1# (0.134) and 2# (0.850). This confirms that the andradite-grossular hydrogarnet in leached Fe-rich RM is the solid solution of 1# and 2#, which are taken as end-member components. Sodalite transforms into cancrinite when exposed to high temperature. The cages of cancrinite's 12-membered ring channels prefer larger cations [24] and thus preferentially select Ca^{2+} over two Na^+s when the former is present in solution as shown in Fig. 5. The final product in this case is $Na_6[Al_6Si_6O_{24}]\cdot 2CaCO_3\cdot nH_2O$ [4].

Fig. 5 shows the effect of various temperatures. The Na_2O content and A/S trends are indicated by the XRD patterns. The relatively high level of Na_2O content and A/S at 200 °C is due to the existence of cancrinite $Na_6Ca_2Al_6Si_6O_{24}(CO_3)_2\cdot 2H_2O$. The cancrinite had disappeared by 240 °C, having transformed into 1# and 2# with Fe_2O_3. Andradite-grossular hydrogarnet was the main crystal phase at each temperature. As temperature increased, its peaks strengthened due to the gradual reduction of A/S and the corresponding rising proportion of 1# grown in the leached RM.

Fig. 6 shows the influence of various sodium concentrations. When sodium concentrations were 196 gpl and 324 gpl, the crystal phases were mainly 1# and 2#. When entering the hydrochemical method region at 433 gpl, $NaCaHSiO_4$ emerged. At this point, the content of Na_2O increased and that of Al_2O_3 began a continuous decline. It is noteworthy that 1# and 2# were still present at 433 gpl, despite having entered the hydrochemical method region. Their presence makes it clear that the variation of Na_2O and A/S essentially depends on the crystal phase change.

3.1.1.3. Effect of caustic ratio. The caustic ratio's effect was also investigated. In accordance with the conditions discussed above, experiments were carried out at 280 °C, Na_2O 283 gpl, and a resi-

Table 3
Chemical compositions of leached Fe-rich RM at various sodium concentrations and the A/S in leached solution[a] (wt%).

	Na_2O	Al_2O_3	Fe_2O_3	SiO_2	CaO	TiO_2	A/S	A/S in leached solution
196 gpl	1.16	6.79	21.39	18.23	28.89	3.46	0.373	42.83
283 gpl	0.49	5.55	22.44	18.73	30.39	3.63	0.297	20.82
324 gpl	0.44	5.69	23.33	19.02	34.07	3.70	0.299	20.65
362 gpl	0.48	5.08	23.09	17.62	30.74	3.71	0.288	14.46
433 gpl	3.01	4.59	23.54	13.10	28.71	3.76	0.350	12.40

[a] Reaction at 280 °C.

Table 4
Chemical compositions of leached Fe-rich RM at various temperatures and the A/S in leached solution[a] (wt%).

	Na_2O	Al_2O_3	Fe_2O_3	SiO_2	CaO	TiO_2	A/S	A/S in leached solution
280 °C	0.44	5.69	23.33	19.02	34.07	3.70	0.299	20.65
260 °C	1.54	7.81	21.38	16.77	27.50	3.40	0.466	36.25
240 °C	3.65	11.11	20.28	15.40	26.73	3.13	0.722	48.32
200 °C	4.43	12.89	18.92	14.25	23.51	2.83	0.905	51.27

[a] Reaction at Na_2O 324 gpl.

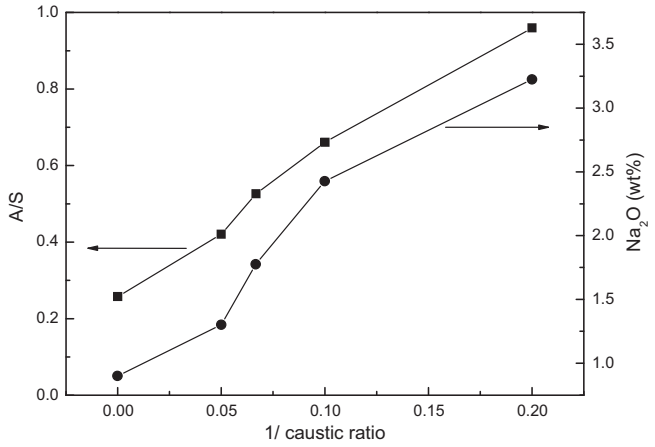

Fig. 7. Na_2O content and A/S in leached Fe-rich RM as a function of caustic ratio.

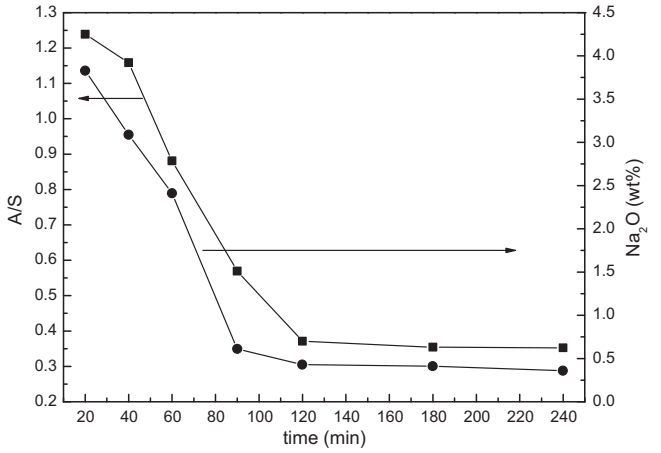

Fig. 8. Na_2O content and A/S in leached Fe-rich RM as a function of residence time.

dence time of 2 h. The results are shown in Fig. 7. As the caustic ratio increased from 5 to infinity over the course of 2 h, the leached RM's Na_2O content and A/S were observed to decrease from 3.23 wt% to 0.90 wt% and from 0.96 to 0.26, respectively.

Despite its effectiveness in recovering alkali and alumina from RM, acquisition of a suitably high caustic ratio solution for industrial manufacturing remains difficult. The use of an inappropriately low caustic ratio solution would lead to unacceptable Na_2O content and A/S results. Overall, this research made use of solutions with a caustic ratio of 20.

3.1.1.4. Effect of residence time. The experiments were performed under the conditions which were 280 °C, Na_2O 324 gpl, caustic ratio of 20. The residence time was taken at the range from 20 min to 240 min. The results are plotted in Fig. 8 and the chemical compositions are displayed in Table 5.

From Fig. 8, it is obviously observed that the Na_2O content and A/S in leached RM decreased rapidly within the residence time ranging from 20 min to 120 min, whereas they changed slightly when residence time was over 120 min. Hence, 2 h of residence time was selected for other experiments as one optimal variable. In addition, the Na_2O content in Fe-rich RM decreased from initial 10.46 wt% to 3.09 wt% in 20 min reaction. The extraction of alkali went faster than that of alumina. This phenomenon can be explained by their XRD patterns shown in Fig. 9.

As the XRD patterns after 2 h are the same as that at 2 h, Fig. 9 just shows the XRD patterns from 20 min to 120 min. As Fig. 9 showed, in 20 min, sodalite had totally disappeared, cancrinite with weak peaks and silicate hydrogarnet with sharp and strong peaks formed. It explained the Na_2O content decreased sharply in initial 20 min. In addition, the early formed silicate hydrogarnet was

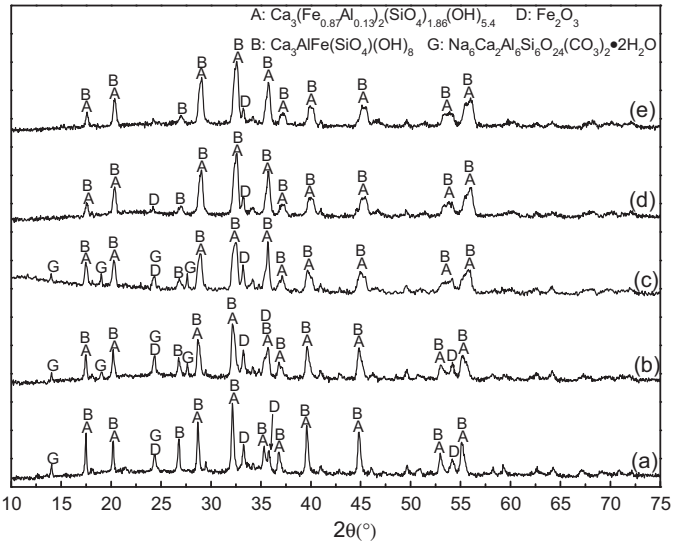

Fig. 9. XRD patterns of leached Fe-rich RM after leaching at 280 °C, Na_2O 324 gpl and different residence times: (a) 20 min, (b) 40 min, (c) 60 min, (d) 90 min, (e) 120 min.

Table 5
Chemical compositions of leached Fe-rich RM at various residence times (wt%).

	Na_2O	Al_2O_3	Fe_2O_3	SiO_2	CaO	TiO_2	A/S
20 min	3.09	17.22	13.91	18.40	25.04	2.98	1.239
40 min	3.83	15.94	13.76	18.05	25.15	2.92	1.158
60 min	2.41	13.24	15.03	20.96	29.49	3.32	0.881
90 min	0.61	8.35	14.68	20.16	29.10	3.14	0.569
120 min	0.43	6.74	18.16	21.42	31.07	3.44	0.371
180 min	0.41	6.32	17.83	21.32	30.83	3.35	0.354
240 min	0.36	6.39	18.13	20.92	30.75	3.41	0.352

Table 6
Chemical compositions of leached Fe-lean RM at various sodium concentrations (wt%).

	Na_2O	Al_2O_3	Fe_2O_3	SiO_2	CaO	TiO_2	A/S
283 gpl	1.65	15.01	5.20	13.50	38.12	4.20	1.112
324 gpl	3.30	12.49	5.21	15.11	35.54	3.92	0.827
362 gpl	4.84	8.64	6.12	15.83	36.43	4.26	0.546

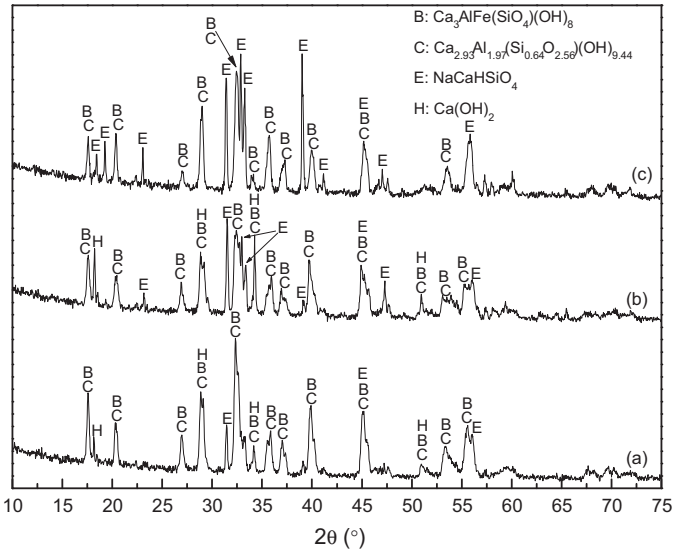

Fig. 10. XRD patterns of leached Fe-lean RM residue after leaching at 280 °C and different sodium concentrations: (a) 283 gpl, (b) 324 gpl, (c) 362 gpl.

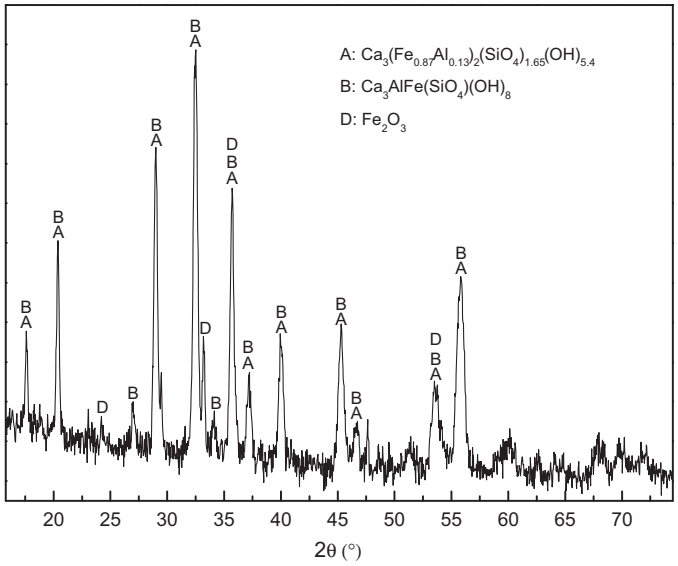

Fig. 11. XRD pattern of leached iron-enriched Fe-lean RM.

mainly grossular hydrogarnet. As reaction proceeded, the hematite peaks got weaken and peaks of garnet got diffuse. It indicated iron got into hydrogarnet to substitute for aluminum and the proportion of andradite in silicate hydrogarnet enhanced. Finally, it formed an andradite-grossular hydrogarnet in which andradite took the main part.

Based on the results above, the optimal reaction conditions are 280 °C, Na_2O 283–362 gpl, caustic ratio 20 and residence time 2 h which was used for the most following reactions.

3.1.2. Dealing with Fe-lean RM

3.1.2.1. Effect of sodium concentration. Fe-lean RM was subjected to three experiments under the optimal conditions identified through Fe-rich RM analysis. The Na_2O content and A/S in leached RM were much higher than those of leached Fe-rich RM, and decreased when the sodium concentration increased as seen in Table 6.

3.1.2.2. Analysis of phases. This trend can be explained by their XRD patterns shown in Fig. 10. The XRD pattern of crystal phase $Ca_{2.93}Al_{1.97}(Si_{0.64}O_{2.56})(OH)_{9.44}$ (3#) is structurally isomorphic with 1# and 2#, and its XRD pattern resembles that of 2#. It is believed that the 2# and 3# are the end-member components of andradite-grossular hydrogarnet in leached Fe-lean RM. The substitution ratio of iron on aluminum is much lower than that of Fe-rich RM, i.e. grossular takes a large proportion of the hydrogarnet, which keeps the A/S high. Decreases in ferric oxide favor the formation of $NaCaHSiO_4$. The XRD patterns show that, as sodium concentration increased, the peaks of 2# and 3# got weaken while those of $NaCaHSiO_4$ were enhanced. It is this reason why Fe-lean RM's Na_2O content and A/S are higher than those of Fe-rich RM despite identical operating conditions.

3.1.2.3. Effect of iron addition. The greatest difference between the two kinds of RM lies in the ferric oxide content. The experiment was repeated with the addition of ferric oxide into the reaction system from an external source in order to verify whether low ferric oxide content was indeed the cause behind high Na_2O content and A/S in leached residue. Considering the alkali nature of the system, ferric hydroxide was chosen for iron enrichment. Post-enrichment, the Fe-lean RM sample's iron content matched that of Fe-rich RM. This experiment was carried out at 280 °C, Na_2O 324 gpl, caustic ratio 20 and residence time 2 h.

Post-enrichment, the Na_2O content was 1.25 wt% and A/S reached 0.454, as shown in Table 7. The XRD pattern in Fig. 11 reveals the total disappearance of $NaCaHSiO_4$ and the emergence of sharp peaks of andradite-grossular hydrogarnet. The existence of iron restrains the phase of $NaCaHSiO_4$ and promotes the substitution of iron on aluminum, both of which facilitate the decrease of Na_2O content and A/S in leached RM. Thus, iron's crucial role in the hydrothermal process is evident. By extension, Fe-lean RM is not suitable for the hydrothermal process unless it is enriched with iron before processing.

3.1.2.4. Blending of Fe-rich & Fe-lean RM. According to the discussion above, it is natural to consider enriching the Fe-lean RM with the addition of Fe-rich RM. To test this, three experiments were carried out with Fe-rich RM addition amounts of 40, 60 and 80 wt% of RM mixture. The reaction was under 280 °C, Na_2O 324 gpl,

Table 7
Chemical compositions of leached Fe-lean RM after adding ferric hydroxide (wt%).

Na_2O	Al_2O_3	Fe_2O_3	SiO_2	CaO	TiO_2	A/S
1.25	5.94	21.24	13.09	31.60	4.58	0.454

Table 8
Chemical compositions of leached Fe-lean RM with Fe-rich RM addition (wt%).

	Na_2O	Al_2O_3	Fe_2O_3	SiO_2	CaO	TiO_2	A/S[TM]
40 wt%	3.14	9.94	13.64	17.25	26.31	4.35	0.576
60 wt%	2.38	8.97	16.53	17.62	26.07	4.11	0.509
80 wt%	1.17	8.32	19.49	17.76	25.32	3.71	0.468

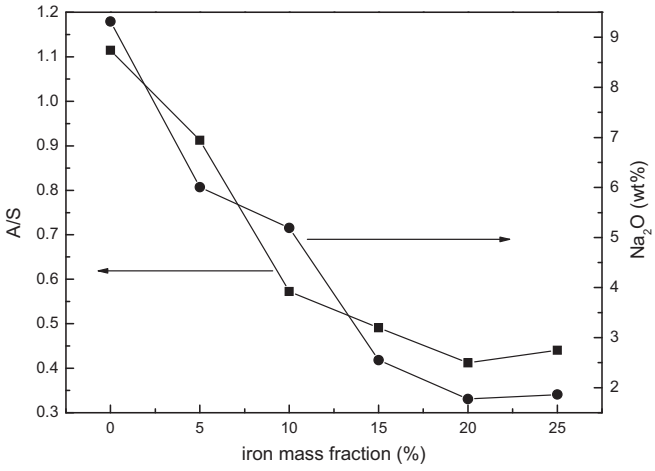

Fig. 12. Effect of iron addition on Na_2O content and A/S.

caustic ratio 20, residence time 2 h and the results are shown in Table 8.

Table 8 shows the Na_2O content and A/S in leached residue decreased as Fe-rich RM amount increased. As expected, the Na_2O content and A/S are between the values of Fe-rich RM and Fe-lean RM under the same reaction condition. Due to the relatively excess iron in Fe-rich RM, the addition of Fe-rich RM promotes the extraction of alkali and alumina in Fe-lean RM to some extent. However, in light that the Fe-lean RM is far from the Fe-rich RM from a geographical viewpoint in China, it is kind of impossible to blend the two species RM for industrial application.

3.2. Effect of ferric compound content and type

3.2.1. Effect of ferric compound content

Having established that iron plays a critical role in the leaching success of the hydrothermal method, it becomes necessary to scrutinize the effectiveness of different amounts of iron. To accomplish this, synthetic sodalite was substituted for RM and six experiments were conducted across a sodalite weight percentage range of 0–25. Ferric hydroxide acted as the iron enrichment source for the alkali reaction system. The reaction conditions were the same as those of RM except the temperature was 260 °C and Na_2O 324 gpl. In addition, in order to better simulate the components of RM, titanium dioxide accounting for 4 wt% of sodalite by weight was added to the system.

As Table 9 and Fig. 12 show, the Na_2O content and A/S in leached residue decreased as the amount of iron enrichment increased, though enrichments past 20 wt% had little effect. Acceptable Na_2O content and A/S can conclusively be achieved through the hydrothermal process provided that the iron content is sufficient. Therefore the Chinese diaspore-RM, i.e. Fe-lean RM with an iron content of 6–8 wt% Fe_2O_3, is not suitable for the hydrothermal process unless there is an additional source of iron.

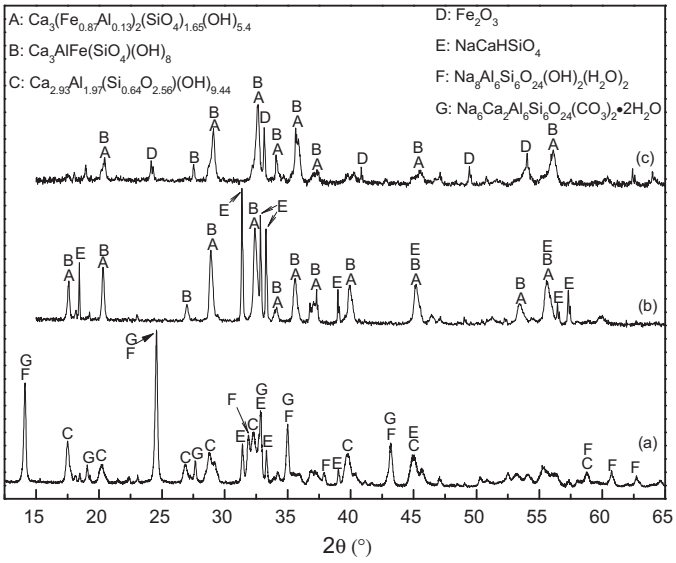

Fig. 13. XRD patterns of leached residue of sodalite with different degrees of iron addition: (a) 0 wt%, (b) 10 wt%, (c) 20 wt%.

As shown in Fig. 13, with inadequate levels of iron, the DSP was not decomposed in 2 h, and there was some $NaCaHSiO_4$ and andradite-grossular hydrogarnet. At 10 wt% iron content, the DSP disappeared and the quantity of $NaCaHSiO_4$ increased. Finally, after increasing iron content to 20 wt%, $NaCaHSiO_4$ disappeared, with andradite-grossular hydrogarnet as the main phase, and some Fe_2O_3 emerged.

3.2.2. Effect of ferric compound type

Iron enrichment of Fe-lean RM is very efficient. However, the type of the ferric compound in Fe-rich RM is uncertain, leaving questions as to the propriety of enrichment with ferric hydroxide. Further research into the type of RM's ferric compounds is needed.

Goethite and hematite are the primary iron minerals present in bauxite, though small amounts of magnetite, chamosite, ilmenite, siderite and pyrite may also be present [19]. These minerals decompose during the bauxite digestion process with the notable exception of hematite. Goethite's conversion into hematite in alkali solutions is well-documented [25,26], and some iron hydrogarnet is

Table 9
Chemical compositions of leached residue of sodalite with ferric hydroxide addition (wt%).

	Na_2O	Al_2O_3	Fe_2O_3	SiO_2	CaO	TiO_2	A/S
0 wt%	9.32	23.40	0.00	21.00	26.29	4.86	1.114
5 wt%	6.01	19.01	5.37	20.84	27.72	5.35	0.912
10 wt%	5.19	11.88	9.57	20.75	26.89	5.03	0.573
15 wt%	2.55	9.12	16.64	18.58	26.98	4.86	0.491
20 wt%	1.77	7.50	22.45	18.19	24.08	5.02	0.412
25 wt%	1.87	7.56	27.81	17.16	22.49	4.61	0.441

Table 10
Chemical compositions of leached residue with different ferric compounds addition (wt%).

	Na_2O	Al_2O_3	Fe_2O_3	SiO_2	CaO	TiO_2	A/S
Fe_2O_3	10.11	19.09	13.50	18.29	19.92	0.00	1.04
$Fe(OH)_3$	2.26	7.35	14.92	18.85	28.76	0.00	0.39

Table 11
Chemical compositions of leached residue with titanium dioxide addition (wt%).

	Na_2O	Al_2O_3	Fe_2O_3	SiO_2	CaO	TiO_2	A/S
Fe_2O_3	2.21	9.70	16.68	18.51	28.17	3.83	0.52
$Fe(OH)_3$	1.96	8.39	15.45	19.24	27.79	4.32	0.44

typically generated by the improved Bayer process. The type of iron in RM should therefore be hematite, iron hydrogarnet, and perhaps some goethite which has not totally converted to hematite.

Excluding iron hydrogarnet as it is the target product, RM's ferric compounds have two morphologies: goethite and hematite. In this study, the reagents ferric hydroxide and ferric oxide were used to represent goethite and hematite, respectively. The reaction conditions were the same as those for RM experiments except the temperature was 260 °C, and the sodium concentration was 284 gpl. Iron enrichment constituted 15 wt% of sodalite, and the dosages of ferric compounds were both based on the molecular formula of Fe_2O_3.

As Table 10 shows, the kind of ferric compound used for enrichment significantly affects the leaching results. However, there is a significant difference in between the results from the ferric oxide enriched residue and ferric hydroxide enriched residue, and the type of ferric compound in Fe-rich RM is hematite. It seems paradoxical that the treatment results of Fe-rich RM are much better than those of synthetic materials with ferric oxide.

The key difference between real RM and the synthetic substitute is the presence of titanium compounds. To correct for this deficiency, the experiments were repeated with the addition of titanium dioxide accounting for 4 wt% of sodalite. The results are shown in Table 11.

The addition of titanium improved treatment via ferric oxide enrichment, while having no significant impact on the results of ferric hydroxide enrichment. The XRD patterns of leached residue with ferric oxide addition are shown in Fig. 14. In the absence of titanium dioxide, the DSP was not decomposed within 2 h, while its presence allowed the andradite-grossular hydrogarnet to become the main phase.

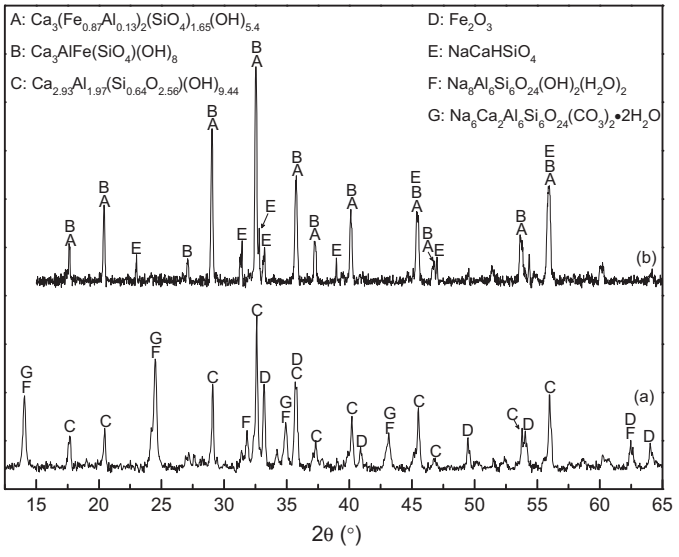

Fig. 14. XRD patterns of leached residue of sodalite with ferric oxide addition: (a) without titanium dioxide, (b) with titanium dioxide.

Hematite is usually the main Fe-bearing phase for Fe-rich red muds such as gibbsite RM. It is apparent that hematite, which could not generate silicate hydrogarnet alone, can be effective with the assistance of titanium. The 2–4 wt% of TiO_2 commonly found in RM is enough to assist hematite in the formation of hydrogarnet. Titanium dioxide can strongly restrain the transformation of goethite to hematite [26], and titanium in alkali solution always combines with calcium to form a series of calcium–titanium compounds [23]. However, it is uncertain whether the titanium compound works as a catalyst or enters the structure of silicate hydrogarnet to facilitate the generation of andradite-grossular hydrogarnet. The mechanism of titanium's assistance needs further study.

4. Conclusions

The hydrothermal process is feasible when dealing with Bayer RM. Under optimal conditions, the Na_2O content and A/S in leached Fe-rich RM could reach 0.5 wt% and 0.3, respectively. Further, after iron enrichment, the Na_2O content and A/S of leached Fe-lean RM can achieve the same levels as those of Fe-rich RM.

The objective phase in the hydrothermal process is andradite-grossular hydrogarnet, which is created through the decomposition of DSP to recover alkali and alumina. In this article, three end-members of andradite-grossular hydrogarnet were used to describe the substitution ratio of iron on aluminum. When the substitution ratio is high, such as with Fe-rich RM, the hydrogarnet is composed of $Ca_3(Fe_{0.87}Al_{0.13})_2(SiO_4)_{1.65}(OH)_{5.4}$ (1#) and $Ca_3AlFe(SiO_4)(OH)_8$ (2#). Similarly, for a low substitution ratio, such as with Fe-lean RM, it is composed of 2# and $Ca_{2.93}Al_{1.97}(Si_{0.64}O_{2.56})(OH)_{9.44}$ (3#). At the same time, the DSP cannot be decomposed within 2 h and some $NaCaHSiO_4$, the effective phase in the hydrochemical process, emerges. This leads to both the Na_2O content and A/S in RM remaining high.

Research was also carried out on the effect of ferric compound content and type on the recovery of alumina and alkali by synthetic materials. The Na_2O content and A/S decrease continuously as the amount of ferric compound increases until the ferric compound accounts for 20 wt% of solid, after which no significant changes occur. In addition, it was discovered that leaching from hematite, as the main Fe-bearing phase in RM, requires the assistance of titanium. The mechanism of assistance of the titanium compound needs further research.

Acknowledgements

We acknowledge financial support from the National Key Basic Research Program of China (973 Program, 2007CB613501), the National Key Technologies R&D Program (2006BAC02A05 and 2009BAC64B03) and Chinese Academy of Sciences Knowledge Innovation Program (KGCX2-YW-321-2).

References

[1] IAI, International Aluminum Institute. http://www.world-aluminium.org/, 2009.
[2] I. Paspaliaris, A. Karalis, The effect of various additives on diasporic bauxite leaching by the Bayer process, Light Met. (1998) 35–39.
[3] W. Liu, J. Yang, B. Xiao, Review on treatment and utilization of bauxite residues in China, Int. J. Miner. Process. 93 (2009) 220–231.
[4] P. Smith, The processing of high silica bauxites – review of existing and potential processes, Hydrometallurgy 98 (2009) 162–176.
[5] S.J. Palmer, B.J. Reddy, R.L. Frost, Characterisation of red mud by UV–vis NIR spectroscopy, Spectrochim. Acta Part A 71 (2009) 1814–1818.
[6] Y. Cengeloglu, E. Kir, M. Ersoz, T. Buyukerkek, S. Gezgin, Recovery and concentration of metals from red mud by Donnan dialysis, Colloids Surf. A 223 (1–3) (2003) 95–101.
[7] B.I. Whittington, B.L. Fletcher, C. Talbot, The effect of reaction conditions on the composition of desilication product (DSP) formed under simulated Bayer conditions, Hydrometallurgy 49 (1998) 1–22.
[8] K. Zheng, R.S.C. Smart, J. Addai-Mensah, A. Gerson, Solubility of sodium aluminosilicates in synthetic Bayer liquor, J. Chem. Eng. Data 43 (1998) 312–317.
[9] M.C. Barnes, J. Addai-Mensah, A.R. Gerson, The mechanism of the sodalite-to-cancrinite phase transformation in synthetic spent Bayer liquor, Microporous Mesoporous Mater. 31 (1999) 287–302.
[10] B.R. Ablamoff, Physical and chemical principles of comprehensive treatment of aluminum-containing raw materials by basic process, Q. Chen (trans.), 1988.
[11] L. Zhong, Y. Zhang, Y. Zhang, Extraction of alumina and sodium oxide from red mud by a mild hydro-chemical process, J. Hazard. Mater. 172 (2009) 1629–1634.
[12] P.J. Cresswell, D.J. Milne, A hydrothermal process for recovery of soda and alumina from red mud, Light Metals (1982) 227–238.
[13] G.A. Lager, J.C. Nipko, C.-K. Loong, Inelastic neutron scattering study of the (O_4H_4) substitution in garnet, Physica B 241–243 (1998) 406–408.
[14] T.B. Ballaran, A.B. Woodland, Local structure of ferric iron-bearing garnets deduced by IR-spectroscopy, Chem. Geol. 225 (2006) 360–372.
[15] F.C. Hawthorne, Some systematics of the garnet structure, J. Solid State Chem. 37 (1981) 157–164.
[16] A.J. Locock, An excel spreadsheet to recast analyses of garnet into end-member components, and a synopsis of the crystal chemistry of natural silicate garnets, Comput. Geosci. 34 (2008) 1769–1780.
[17] R.H. Nobes, E.V. Akhmatskaya, V. Milman, B. Winkler, C.J. Pickard, Structure and properties of aluminosilicate garnets and katoite: an ab initio study, Comput. Mater. Sci. 17 (2000) 141–145.
[18] S.J. Marin, M. O'Keefee, The crystal structure of the hydrogarnet $Ba_3In_2(OD)_{12}$, J. Solid State Chem. 87 (1990) 173–177.
[19] J. Zoldi, K. Solymar, J. Zambo, M.K. Jonas, Iron hydrogarnets in the Bayer process, in: Proceedings of TMS Light Metals, 1987, pp. 105–111.
[20] X. Li, S. Gu, Z. Yin, G. Wu, Y. Zhai, Regulating the digestion of high silica bauxite with calcium ferrite addition, Hydrometallurgy (2010).
[21] K. Solymar, J. Steiner, J. Zoldi, Technical peculiarities and viability of hydrothermal treatment of red mud, in: Proceeding of TMS Light Metals, 1997, pp. 49–54.
[22] F.C. Hawthorne, The use of end-member charge-arrangements in defining new mineral species and heterovalent substitutions in complex minerals, Can. Miner. 40 (2002) 699–710.
[23] L. Xiao-bin, F. Wei-an, Z. Qiu-sheng, L. Gui-hua, P. Zhi-hong, Reaction behavior and mechanism of anatase in digestion process of diasporic bauxite, Trans. Nonferrous Met. Soc. China 20 (2010) 142–146.
[24] E. Jordan, R.G. Bell, D. Wilmer, H. Koller, Anion-promoted cation motion and conduction in zeolites, J. Am. Chem. Soc. 128 (2006) 558–567.
[25] S. Shaw, S.E. Pepper, N.D. Bryan, F.R. Livens, The kinetics and mechanisms of goethite and hematite crystallization under alkaline conditions, and in the presence of phosphate, Am. Miner. 90 (2005) 1852–1860.
[26] J. Murray, L. Kirwan, M. Loan, B.K. Hodnett, In-situ synchrotron diffraction study of the hydrothermal transformation of goethite to hematite in sodium aluminate solutions, Hydrometallurgy 95 (2009) 239–246.